The Penetration of Draped Magnetic Field Into the Martian Upper Ionosphere and Correlations With Upstream Solar Wind Dynamic Pressure

C. M. Fowler, C. O. Lee, S. Xu, D. L. Mitchell, R. Lillis, T. Weber, J. Halekas, L. Andersson, J. Espley, R. E. Ergun, et al.

AGU100 ADVANCING EARTH AND SPACE SCIENCE

JGR Space Physics

RESEARCH ARTICLE
10.1029/2019JA026550

Key Points:
- Four years of MAVEN data are analyzed to investigate the penetration of draped magnetic field into the Martian upper ionosphere
- The upper extent of the Martian ionosphere coincides with the transition from closed to open and draped magnetic field topologies
- Open and draped magnetic field topologies are observed at lower altitudes during higher solar wind dynamic pressure conditions

Correspondence to:
C. M. Fowler,
cmfowler@berkeley.edu

Citation:
Fowler, C. M., Lee, C. O., Xu, S., Mitchell, D. L., Lillis, R., Weber, T., et al. (2019). The penetration of draped magnetic field into the Martian upper ionosphere and correlations with upstream solar wind dynamic pressure. *Journal of Geophysical Research: Space Physics*, *124*, 3021–3035. https://doi.org/10.1029/2019JA026550

Received 25 JAN 2019
Accepted 20 MAR 2019
Accepted article online 27 MAR 2019
Published online 8 APR 2019

The Penetration of Draped Magnetic Field Into the Martian Upper Ionosphere and Correlations With Upstream Solar Wind Dynamic Pressure

C. M. Fowler[1], C. O. Lee[1], S. Xu[1], D. L. Mitchell[1], R. Lillis[1], T. Weber[2], J. Halekas[3], L. Andersson[2], J. Espley[4], R. E. Ergun[2], C. Mazelle[5], and J. Luhmann[1]

[1]Space Sciences Laboratory, University of California, Berkeley, CA, USA, [2]Laboratory of Atmospheric and Space Sciences, University of Colorado Boulder, Boulder, CO, USA, [3]Department of Physics And Astronomy, University of Iowa, Iowa City, IA, USA, [4]NASA Goddard Space Flight Center, Greenbelt, MD, USA, [5]IRAP, University of Toulouse-CNRS-UPS-CNES, Toulouse, France

Abstract Open and draped magnetic field topologies are important at Mars because they can provide ionospheric particles a path to escape to space. Four years of Mars Atmosphere and Volatile EvolutioN data are analyzed in this study, demonstrating that the altitude at which the ionospheric density drops below 10^2 cm^{-3} is essentially coincident with the altitude down to which open and draped magnetic field lines are observed in the ionosphere. During times of enhanced solar wind dynamic pressure, a greater fraction of the magnetic topology was observed as open or draped (as opposed to closed) above densities of 10^2 cm^{-3}. The altitudes at which the ionospheric density fell below 10^2 cm^{-3}, and the magnetic field topology transitioned from closed to open or draped, also decreased during higher dynamic pressure conditions. Times of enhanced solar wind dynamic pressure thus appear to drive greater penetration of draped magnetic field into the ionosphere, enhancing the rate of reconnection between draped and crustal magnetic fields and producing more open field. Such observations may have implications for the long-term evolution of the Martian ionosphere; the historic solar wind is thought to have been denser and faster than present-day conditions, and "quiet time" conditions may have been equivalent to extreme dynamic pressure events today. Depending on past atmospheric conditions at Mars, draped topology may have routinely penetrated deep into the ionosphere, and quiet time rates of ionospheric escape to space may thus have been much greater for early Mars than today.

1. Introduction

Mars lacks an internally driven dipole magnetic field, and consequently, the interaction between the planet, its ionosphere and extended exosphere, and the supersonic solar wind results in the formation of a partially induced magnetosphere (e.g., Bertucci et al., 2011; Brain et al., 2003; Halekas et al., 2017a). The mixed nature of the Martian magnetosphere, where particle thermal pressure and magnetic pressure are both significant contributors to standing off the solar wind, also leads to a highly variable magnetic environment that can influence plasma interactions, particularly on the dayside of the planet. This variability is driven in large part by upstream solar wind conditions. Such behavior is different at magnetized planets, for example, Earth, where the strong dipole magnetic field dominates in the interaction with the super sonic solar wind flow and produces a much more "rigid" obstacle.

The highly variable magnetic environment in the Martian magnetosphere can lead to significant and sudden changes in the local magnetic field strength, orientation, and topology, which can occur on timescales less than the ion gyroperiod. Of particular interest in this study is the local magnetic field topology, which describes the plasma regions to which the local magnetic field is connected. Three types of topology have been identified at Mars: (1) draped magnetic fields that have both ends of the local field line embedded within the solar wind; (2) open magnetic fields that have one end of the local field line embedded within the solar wind and the other end embedded below the electron exobase region deep within the ionosphere (the electron exobase is typically defined as the region where the electron mean free path is equal to the ionospheric scale height, and is usually located at around 160 km altitude [Xu et al., 2015]); and (3) closed magnetic field lines that have both ends of the local field line embedded below the electron exobase region.

Draped field lines are a result of the interplanetary magnetic field encountering the planetary obstacle as they are advected along with the solar wind flow. The formation of draped field lines begins upstream of the Martian bow shock; the photoionization and charge exchange of exospheric neutrals there leads to "mass loading" of the solar wind when these newly produced ions are accelerated by the solar wind motional electric field. Conservation of momentum subsequently reduces the solar wind flow velocity upstream of the planet (e.g., Breus et al., 1989; Dubinin & Lundin, 1995; Chaffin et al., 2015; Holmström, 2006; Rahmati et al., 2015). Downstream of the bow shock, solar wind magnetic fields penetrate into the dayside Martian ionosphere, where additional induced ionospheric currents (produced as a result of the finite conductivity of the Martian ionosphere) cause them to appear "hung up" in the dayside ionosphere. Both ends of these field lines remain embedded within the solar wind on either side of the planetary obstacle; advection of these ends with the solar wind flow past the planet results in the formation of induced magnetotail fields in the wake of the planet.

Closed magnetic fields are typically associated with crustal remanent magnetism that is strongest in the Southern Hemisphere (e.g., Acuna et al., 1999). These crustal fields, which rotate with the planet, form "mini magnetospheres" in the ionosphere that can temporarily trap plasma via the Lorentz force.

Open magnetic field lines can form as a result of magnetic reconnection, for example, between draped and closed magnetic fields. Because the upstream solar wind conditions (including solar wind magnetic field orientation) can change on short timescales, and because the crustal magnetic fields rotate with the planet, the global magnetic topology at Mars constantly changes with time.

Above the Martian exobase region (the exobase is typically defined as the altitude where the mean free path equals the atmospheric scale height and is located at around 170–200 km at Mars [Jakosky et al., 2017]), the plasma environment is collisionless, meaning that charged particles will gyrate unimpeded about the local magnetic field in response to the Lorentz force. When draped magnetic field lines penetrate down in to this collisionless region, they provide ionospheric particles access to the solar wind. Open field lines by definition provide ionospheric particles access to the solar wind. Draped and open magnetic field topologies can thus enable direct ionospheric escape to space, assuming that the charged particles possess escape energy to overcome Mars' gravitational potential, and their motion is unhindered by other processes. In contrast, ionospheric particles gyrating about closed magnetic field lines are unlikely to escape to space unless they experience additional physical processes (such as drifts) that shift their guiding center to an open or draped magnetic field line. A closed field line can also become open if conditions cause it to reconnect with other open or draped field.

The above definitions mean that draped and open magnetic field lines are particularly important in the context of ionospheric escape at Mars, and the extent to which they occupy the collisionless regime of the ionosphere is likely to have important implications for enabling such escape. Because the upstream solar wind conditions drive the interaction with the Martian obstacle, "extreme" space weather events, such as coronal mass ejections (CMEs) and high pressure pulses from solar wind stream interactions, have been observed to drastically alter the Martian magnetosphere and drive substantial enhancements of ionospheric escape to space (Curry et al., 2015; Edberg et al., 2010; Futaana et al., 2008; Jakosky et al., 2015a; Luhmann et al., 2017; Lundin et al., 2008; Ma et al., 2014; Ma et al., 2017; Opgenoorth et al., 2013). Recent studies by Xu et al. (2019) and Xu, Fang, et al. (2018) investigated the response of magnetic topology driven by the arrival of CMEs at Mars in 2003 and 2017, respectively, showing that draped magnetic field lines were observed at much deeper altitudes in the ionosphere compared to the quiet time conditions prior to the arrival of each CME. The authors postulated that extreme space weather events may thus expose a greater portion of the Martian ionosphere to open and draped field lines, contributing to the previously reported enhancements of ionospheric escape rates in the aforementioned studies.

The work reported in this paper is a statistical analysis of magnetic topology above the exobase that utilizes 4 years of Mars Atmosphere and Volatile EvolutioN (MAVEN) upstream solar wind data to demonstrate and confirm the importance of draped magnetic fields in enabling ionospheric escape to space. The extent of the upper ionosphere was determined for the locations where open or draped field lines penetrated into the ionosphere. Times when open or draped field lines were observed at lower altitudes in the ionosphere were associated with times of enhanced solar wind dynamic pressure normal to the atmosphere, lending further support to the idea that the occurrences of high solar wind dynamic pressures enable significantly enhanced

ionospheric escape to space at Mars. This study expands on the single CME case studies by Xu et al. (2019) and Xu, Fang, et al. (2018) and demonstrates a general trend is present for all values of solar wind dynamic pressure.

The remainder of this paper is organized as follows: Descriptions of the data sets used in this study are given in section 2; the statistical analysis method is described in section 3, and the results of this study are presented in section 4. Discussion of these results is given in section 5, before concluding in section 6.

2. Data

Data used in this study are taken by the MAVEN mission, which has been operating at Mars since late 2014. MAVEN is in a 4.5-hr elliptical orbit with a typical periapsis altitude of around 150 km and an apoapsis altitude of ~6,400 km (Jakosky et al., 2015b). MAVEN thus samples below the exobase region on each periapsis pass but does not always observe the ionospheric peak, which is located at around 125-km altitude close to the subsolar point.

MAVEN's orbit precesses over time such that the spacecraft periapsis samples all local times and latitudes, including dayside and nightside. The data set analyzed in this study spans from 1 January 2015 to 31 October 2018. Only orbits where periapsis was located at solar zenith angle (SZA) <90° were analyzed, providing a total of 4,188 orbits. Data from the Magnetometer (MAG), Langmuir Probe and Waves (LPW), Solar Wind Electron Analyzer (SWEA), and Solar Wind Ion Analyzer (SWIA) instruments were analyzed.

MAG consists of two fluxgate magnetometers that measure the 3-D magnetic field vector at 32 Hz. The use of two fluxgates provides hardware redundancy and also allows for the calibration and removal of spacecraft generated magnetic fields. More information concerning MAG can be found in Connerney et al. (2015).

Two Langmuir Probes, each mounted at the end of ~7-m booms, and separated by an angular distance of 110°, constitute the LPW instrument. Data from LPW's Langmuir Probe operation mode are analyzed in this study. In this mode, the instrument measures current-voltage (I-V) curves, from which the local ionospheric electron density (N_e), temperature (T_e) and spacecraft potential are derived via the fitting method discussed in Ergun et al. (2015). Derived N_e are analyzed in this study, during times when the spacecraft potential was >−6 V. MAVEN infrequently flies through periapsis in an attitude that causes much larger (absolute) values of spacecraft charging (i.e., <−6 V), during which times the derived values of N_e are less reliable; such times are not included in this study but comprise a small fraction of the total MAVEN LPW data set. Additional information about the LPW instrument can be found in Andersson et al. (2015). Data from the waves operation mode are not analyzed in this study, but the operation and data caveats of this mode are discussed in detail in Fowler et al. (2017).

SWEA consists of a hemispherical top hat electrostatic analyzer whose field of view (360° × 120°) is provided by electrostatic deflectors. SWEA measures electron fluxes from 3 eV up to 5 keV with an energy resolution of 17%. Further information on SWEA can be found in Mitchell et al. (2016). Magnetic topology information can be deduced using a combination of SWEA and MAG data using the method outlined in Xu, Weber, et al. (2018). Topology is inferred from the presence of loss cones (Brain et al., 2007; Weber et al., 2017) and/or ionospheric photoelectrons (Xu et al., 2017). Seven distinct magnetic topologies can be distinguished using this method, encompassing various combinations of closed, open, or draped fields that connect to the dayside and/or nightside ionosphere. The number of topology cases was simplified in this study by combining these groups into two bins: closed field lines, which likely inhibit ionospheric escape to space, and open or draped field lines (termed simply *open* for the remainder of this study), which likely enable ionospheric escape to space.

SWIA is an electrostatic top hat analyzer with a field of view spanning 360° × 90°. Ion fluxes from 25 eV up to 25 keV in energy are measured with an energy resolution of 14.5%. Additional information on SWIA can be found in Halekas et al. (2015a). This study also utilizes averaged upstream solar wind density and velocity information, which is calculated from SWIA data; the method used to calculate these averages is described in Halekas et al. (2017b). These parameters are used to calculate the average upstream solar wind dynamic pressure, $P_{dyn} = m_p n_p v_p{}^2$, where m_p is the proton mass, n_p is the average upstream proton density, and v_p is the average upstream proton velocity. We neglect the dynamic pressure contribution from solar wind alphas, which is typically negligible at Mars, as discussed in Zhang and Luhmann (1992), for example. Depending upon MAVEN's orbit, the spacecraft does not always sample the undisturbed upstream solar wind, and for such orbits, the upstream dynamic pressure can sometimes be calculated based on solar wind protons that

are observed in the dayside ionosphere due to charge exchange with the neutral Martian exosphere (Halekas et al., 2015b). The combination of both techniques provides estimates of the upstream solar wind dynamic pressure during most dayside periapsis passes in the MAVEN data set.

3. Analysis Method and Example Periapsis Profiles

This section discusses the general analysis method used to produce the statistical results shown in section 4. Each of the 4,188 individual periapsis passes comprising the MAVEN data set was assigned a corresponding upstream solar wind dynamic pressure (P_{dyn}) value (whose derivation is discussed in section 2). Because MAVEN's orbit period is approximately 4.5 hr long, data are typically measured in the upstream solar wind ~2–3 hr prior to or after a given periapsis pass. For this study, upstream P_{dyn} values were only paired to a periapsis pass if they occurred within 2.5 hr of the time of periapsis. If these criteria were not met, then a value was not assigned. This method assumes that P_{dyn} does not vary significantly over timescales of less than 2.5 hr, which is not always true; however, it is the best one can do with single spacecraft measurements. An autocorrelation study carried out by Marquette et al. (2018) demonstrated that the typical quiet time values of upstream dynamic pressure at Mars (~7–8 nPa), are observed to vary by 0.1 to 0.2 nPa over a time span of 2.5 hr. For periapsis passes where an upstream P_{dyn} measurement was not available, observations of penetrating protons in the ionosphere, if present, were used to estimate P_{dyn}.

MAVEN data from two example inbound passes are shown in Figure 1, from passes where the contribution from the crustal magnetic anomalies were deemed small. Only passes where the average modeled crustal magnetic field strength from the Morschhauser spherical harmonic model (Morschhauser et al., 2014) was less than 5 nT, across the altitude range 390–410 km, were analyzed in this study. The crustal magnetic anomalies are known to create an even more complex plasma environment, and we focus here on the simplest cases, when such fields are assumed not present.

Data from an inbound pass are shown in Figures 1A–1D, spanning a time range 19 September 2015/06:59:00 to 19 September 2015/07:15:14 UTC. Data from a different inbound pass are shown in panels E–H, spanning a time range of 12 November 2017/16:19:45 to 12 November 2017/16:36:08 UTC. The spacecraft SZA is shown as a function of altitude in panels A and E. Note that negative SZA denote the dawn side of Mars, and positive SZA denote the duskside. The corresponding solar wind dynamic pressure at normal incidence to the atmosphere (referred to as *normal dynamic pressure* for the remainder of this paper) is shown as a function of altitude in panels B and F. This value is obtained by multiplying the upstream solar wind dynamic pressure with the cosine of the spacecraft SZA, squared, at each altitude data point, as done in Zhang and Luhmann (1992), for example. This method assumes that the outer surface of the ionosphere follows a spherical shape as a function of SZA. The SWEA magnetic topology code is shown in panels C and G; a value of 1 denotes that the local magnetic field line is closed, and a value of 2 denotes that the local magnetic field line is either open or draped (termed just *open* for the remainder of this paper). A value of 0 means that the automated code was unable to determine the magnetic field topology: These data points are excluded from any further analysis in this study. The ionospheric electron density, N_e, as derived from LPW measurements, is shown in panels D and H. The vertical blue lines show the average N_e spanning 50-km altitude bins. The horizontal green line ("density threshold 1") denotes where the average N_e falls below 10^2 cm^{-3}; the horizontal dashed orange line ("density threshold 2") denotes where the average N_e falls below 10^3 cm^{-3}. The altitudes at which these density thresholds are observed at are used to parameterize the extent of the upper Martian ionosphere in this study. The choice of these density thresholds is somewhat arbitrary, but they allow us to characterize the extent of the upper ionosphere in a simple manner. The LPW instrument was designed to measure the dense, dayside ionosphere, and uncertainties in derived densities can become larger at densities less than about 10^2 cm^{-3}, which was taken into consideration when specifying these density thresholds.

During the pass from 19 September 2015, MAVEN starts close to the subsolar point at high altitudes and moves to higher SZA as the spacecraft approaches periapsis (panel A). Subsequently, the solar wind dynamic pressure normal to the atmosphere decreases as MAVEN approaches periapsis due to its dependence on cosine(SZA)^2 (panel B). A sharp, almost "ledge-like" cutoff is observed in the density profile at about 400-km altitude, with density thresholds 1 and 2 separated by only 50 km in altitude (panel D). This feature coincides with the lowest altitudes that open magnetic field topology is observed down to, marked by the red dashed horizontal line in panel C.

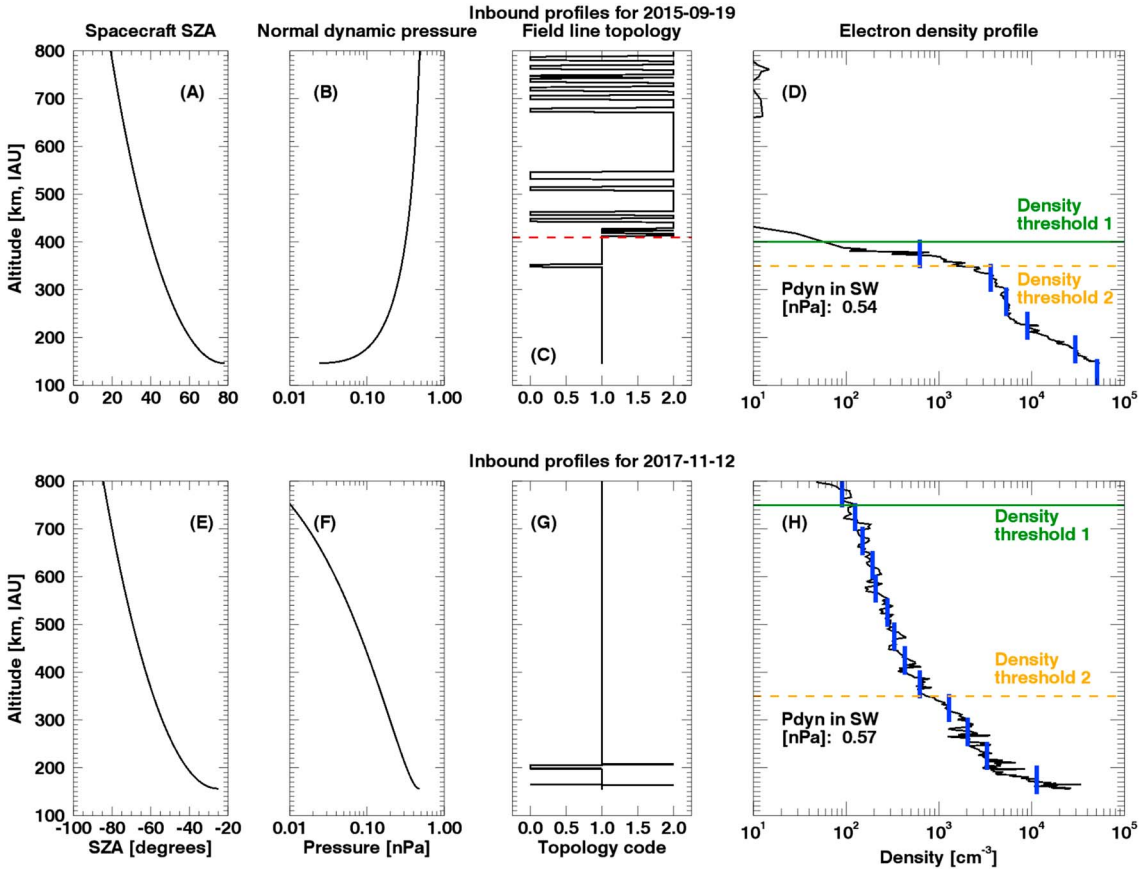

Figure 1. Example profiles from two different inbound MAVEN passes. The spacecraft SZA during each pass is shown in panels A and E (positive for dusk and negative for dawn); the corresponding solar wind dynamic pressure is shown in panels B and F; the magnetic field topology is shown in panels C and G (0 = unknown, 1 = closed, and 2 = open); the ionospheric electron density is shown in panels D and H. The vertical blue lines show the average density over 50-km altitude bins; the solid green and dashed yellow lines mark the altitudes of density thresholds 1 and 2, respectively; the dashed red line in panel C marks the topology transition altitude. SW = solar wind; SZA = solar zenith angle.

During the pass from 12 November 2017, MAVEN is close to the dawn terminator at high altitudes and approaches the subsolar point as it travels toward periapsis (panel E). The corresponding solar wind dynamic pressure normal to the atmosphere increases closer to periapsis (panel F). The observed density profile is qualitatively very different to the one shown in panel D. The profile shown in panel H decreases much more smoothly with altitude and extends above 800 km. The sharp ledge-like cutoff in density is not observed, and the density thresholds are separated by a much greater altitude distance. Panel G shows that no open magnetic field topology is observed below 800-km altitude for this pass.

Although we only show two example profiles in Figure 1, we have inspected a much larger number by hand during our analysis. As is discussed later in this section, density and magnetic topology profiles can demonstrate large orbit-to-orbit and interorbit variability. The examples shown in Figure 1 are fairly "neat" and clear-cut, in that the density thresholds are crossed only once and are easily identified and a clear transition from closed to open magnetic field topology occurs as a function of altitude (for Figure 1C). It should be noted that there are also profiles where this is not the case: Localized density bite outs can occur where depletions in density can fall below 10^2 or 10^3 cm^{-3} over altitude ranges of a few hundred kilometers or less, and the magnetic topology can be highly variable, alternating back and forth between open, closed, and unknown topology. For these cases, the lowest altitude at which each density threshold is first passed is used in subsequent analysis. Some of these cases are likely because MAVEN possesses a significant horizontal velocity component through periapsis and such cases are highlighting horizontal spatial structure that MAVEN is flying through. Other cases may be caused by time variability in the Martian magnetosphere and ionosphere, driven by rapidly changing upstream solar wind conditions, for example. We have not investigated the cause of these highly variable cases further, but it is important to note that such cases exist. As is

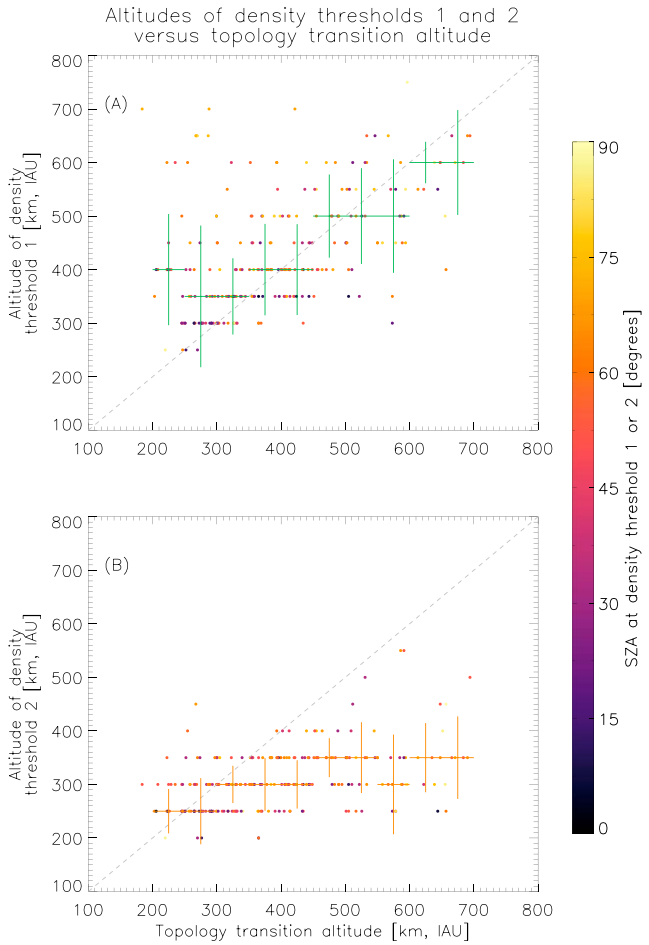

Figure 2. Altitudes of density thresholds 1 and 2 (panels A and B, respectively) as a function of topology transition altitude. Color represents SZA at the altitude of each density threshold. The crosses show the average data when binned: The horizontal bars denote the bin size, and the vertical bars denote the standard deviation within each bin. SZA = solar zenith angle.

shown in later figures, clear statistical trends still appear when the large data set is considered, despite the highly variable nature that may be observed on single periapsis passes.

The results of the statistical analysis, presented in section 4, are obtained through the analysis of the various parameters shown in Figure 1, namely, the altitudes of density thresholds 1 and 2, the altitude at which the magnetic field transitions from predominantly closed to open topology (referred to as the *topology transition altitude* for the remainder of this study), and the incident P_{dyn} at these three altitudes. After passing various data quality filters over the original data set of 8,376 inbound and outbound passes (4,188 orbits), a total of 2,446 inbound and outbound passes were identified for analysis. These quality filters removed times when one or more necessary data products were unavailable, times when spacecraft charging was large (see section 2), times when upstream P_{dyn} values were unavailable, and times when the contribution to the local magnetic field from the localized crustal magnetic anomalies was large.

The altitudes of density thresholds 1 and 2 were determined using an automated algorithm that identifies when the averaged, binned density profiles (the vertical blue lines in Figures 1D and 1H) dropped below 10^2 and 10^3 cm^{-3}. Passes where these drop-offs in density occurred above an altitude of 800 km were not included in the analysis presented here. We attempted to design an automated algorithm that could identify the topology transition altitude in the ionosphere, but this proved difficult due to the variable nature of the topology itself and the fact that magnetic topology cannot always be identified from SWEA and MAG data. We thus inspected 500 random inbound or outbound passes and marked the altitude by hand where the topology transitioned from predominantly closed to open. Topology transitions were only marked for clear-cut cases similar to those shown by the red dashed horizontal line in Figure 1C. For less clear cases, an altitude was omitted. We inspected only the magnetic topology profiles and did not include the corresponding density profiles, so as not to be biased by any features observed in the density profiles. Of the 500 random passes inspected, we were able to mark 249 topology transitions, with the remaining 251 being omitted. Subsequently, analysis presented in section 4 involving the topology transition altitude consists of this data subset of 249 points. All other analyses pertaining to the altitudes of density thresholds 1 and 2 are composed of the 2,446 inbound or outbound passes described above.

4. Results From the Statistical Study

4.1. The Influence of Open Magnetic Field Topology on the Altitudes of Density Thresholds 1 and 2

The altitudes of density thresholds 1 and 2 are shown as functions of the topology transition altitude in Figure 2. Panel A shows the altitudes of density threshold 1, and panel B, the altitudes of density threshold 2. Each data point represents a single inbound or outbound pass from the data subset described at the end of section 3, where the color of each data point is coded with respect to the SZA at each density threshold altitude. The dashed gray line in each panel shows the 1:1 line, where the density threshold altitude equals the topology transition altitude. The green crosses show the statistical properties of the data in panel A when binned into 50-km bins across the horizontal axis (i.e., binned by topology transition altitude). The horizontal bar of each cross marks the horizontal extent of each bin, with its *y* axis value marking the mean density threshold altitude within that bin. The vertical extent of the bar shows the standard deviation of the threshold altitudes within that bin. The orange crosses are the same, but for density threshold 2 altitudes, in panel B.

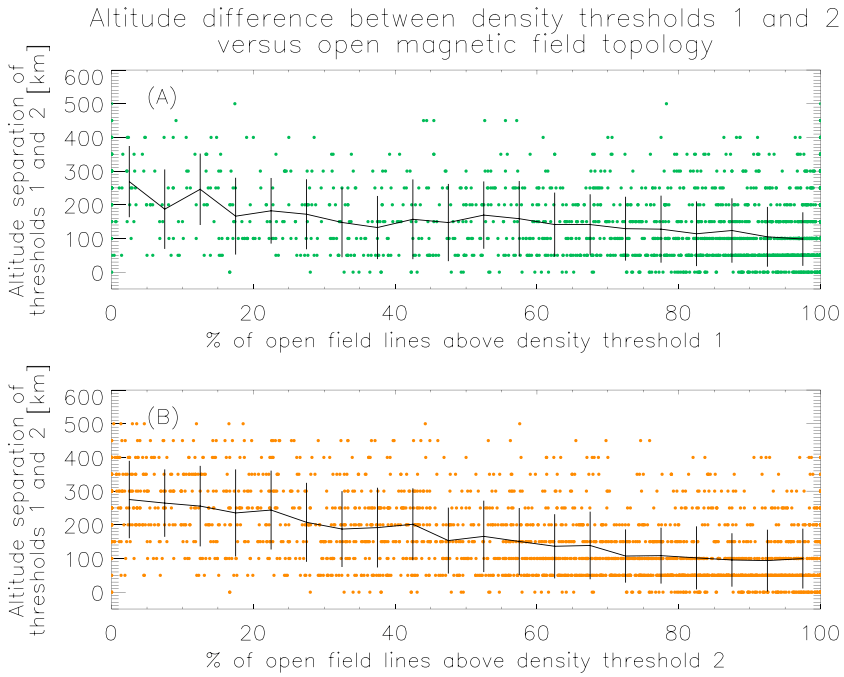

Figure 3. The separation altitude between density thresholds 1 and 2, as a function of the percentage of open magnetic field lines above thresholds 1 and 2 (panels A and B, respectively). The black lines denote the average values when data are binned into horizontal bins 5% wide, with the vertical bars showing the standard deviation within each bin.

Although there is a fair amount of variability shown in panel A, there is a clear, almost 1:1 trend, between the altitude of density threshold 1 and the topology transition altitude. The altitude of density threshold 2 (panel B) does not seem to depend as strongly on the topology transition altitude, and the variability within each bin is significantly smaller than for density threshold 1, especially at lower topology transition altitudes below ~500 km or so. The altitudes of density threshold 1 show a dependence on SZA, in that density threshold 1 is observed at lower altitudes for lower SZA values. A similar trend is present for the altitude of density threshold 2 but to a lesser extent.

The separation distances between the altitudes of density thresholds 1 and 2, as a function of the percentage of open magnetic field lines observed above each threshold, are shown in Figure 3. The horizontal axes in Figure 3 show the percentage of open magnetic field lines above density thresholds 1 and 2. A value of 100% means that all of the magnetic topology above density threshold 1 or 2 was deemed open; a value of 0% means that none of the magnetic field above density thresholds 1 or 2 was open and was 100% closed (we exclude times when the topology code is 0 in this study, so that the sum of the percentage of closed and open field lines is equal to 100%). The solid lines shows the average separation distance for the data, binned in 5% increments, and the vertical bars show the standard deviation within each bin. Significant variability is observed, but as the percentage of open field lines above each density threshold increases, the separation distance between the two thresholds tends to decrease. This trend is clearer for panel B than for panel A.

4.2. The Influence of Solar Wind Normal Dynamic Pressure on the Altitudes of Density Thresholds 1 and 2

The altitudes of density thresholds 1 and 2 as a function of P_{dyn} at each threshold altitude are shown in Figure 4. The data points are colored as a function of SZA at the altitude of density threshold 1 or 2, clearly demonstrating that P_{dyn} tends to decrease as SZA increases, as expected due to the cosine(SZA)^2 dependence of P_{dyn}. To account for this SZA dependence, the data have been binned into nine overlapping SZA bins, centered at 0° to 80° in 10° increments. Each bin spans an SZA range of ±10° from the center SZA value. The solid lines in each figure represent the average values within each SZA bin and show a clear trend that the threshold altitudes decrease as P_{dyn} increases. At least five data points were required to lie within any given bin for an average to be plotted to ensure reasonable counting statistics.

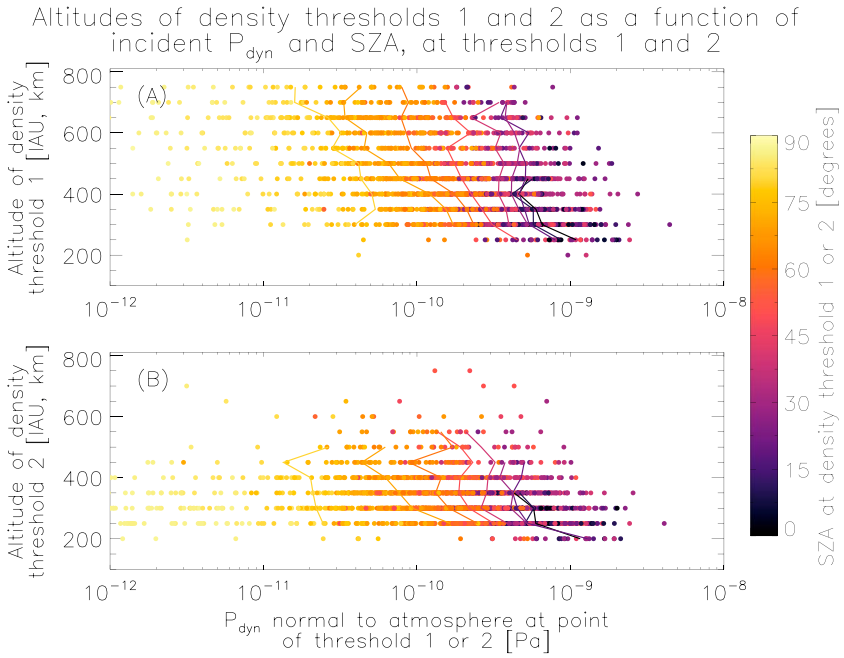

Figure 4. Altitudes of density thresholds 1 and 2 (panels A and B, respectively) as a function of incident dynamic pressure at each threshold. Color denotes SZA at each cut. The solid lines show averages of data binned into overlapping 20°-sized SZA bins, with each bin centered at SZA values of 0° to 80° and spaced every 10°. SZA = solar zenith angle.

The separation distances between density thresholds 1 and 2, as a function of incident P_{dyn} and SZA at density threshold 1, are shown in Figure 5. The data points are again color coded as a function of SZA, and the data have been binned using the same method as in Figure 4 to account for the SZA dependence of P_{dyn}. The solid lines show that the average altitude separation distance between density thresholds 1 and 2 tends to decrease as incident P_{dyn} increases, particularly for values of SZA above ~50°.

4.3. The Influence of Solar Wind Normal Dynamic Pressure on Open Magnetic Field Topology in the Ionosphere

The topology transition altitude, as a function of incident P_{dyn} at that altitude, is shown in Figure 6, where data points are color coded by the SZA at the topology transition altitude. Because this data subset consists

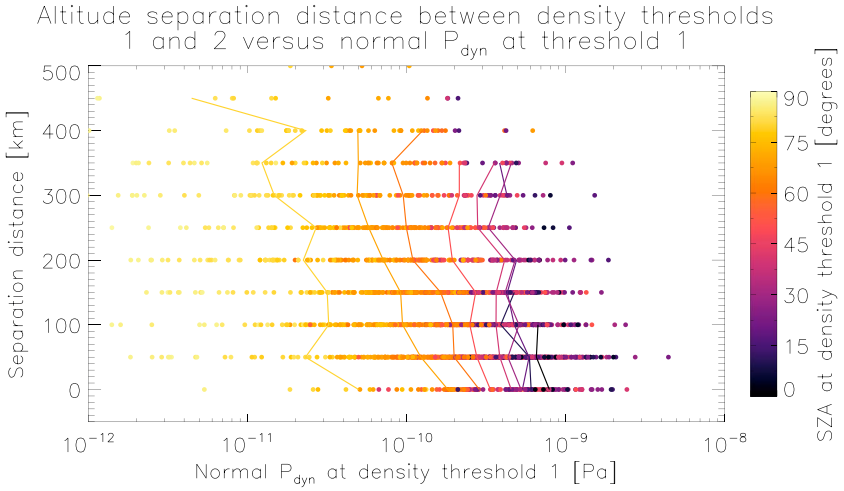

Figure 5. Separation altitude of density thresholds 1 and 2 as a function of incident dynamic pressure at threshold 1. Color denotes SZA at threshold 1. The solid lines show averages of data binned into overlapping 20°-sized SZA bins, with each bin centered at SZA values of 0° to 80° and spaced every 10°. SZA = solar zenith angle.

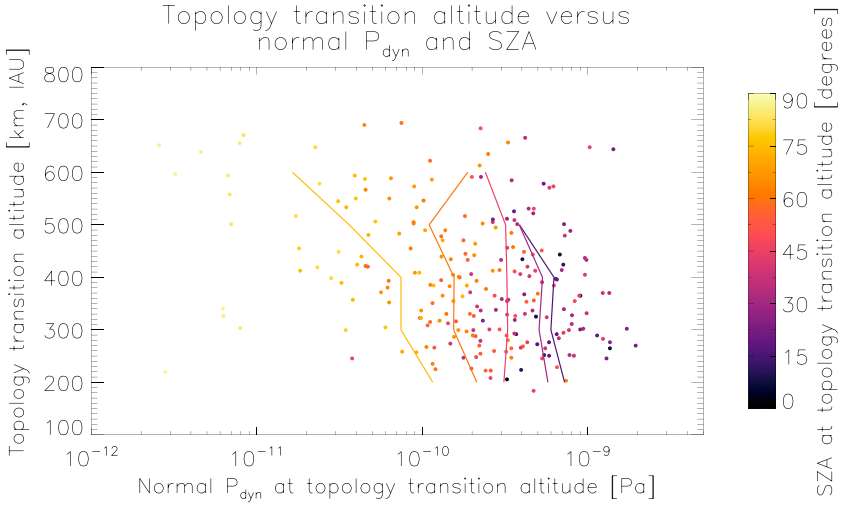

Figure 6. Topology transition altitude as a function of incident dynamic pressure at that altitude. Color denotes SZA at the topology transition altitude. The solid lines show averages of data binned into overlapping 30°-sized SZA bins, with each bin centered at SZA values of 0° to 60° and spaced every 15°. SZA = solar zenith angle.

of fewer points, larger (still overlapping) SZA bin sizes have been used when calculating the averages shown by the solid lines. Bins are centered at SZA values of 0° to 60°, centered every 15° and spanning ±15°. A minimum of three data points were required to plot an average in any given bin. There is significant variability observed for all values of SZA; however, the average values demonstrate that the topology transition altitude tends to decrease with increasing incident P_{dyn}.

The percentage of open magnetic field lines above density thresholds 1 and 2 (up to 800-km altitude) is shown as a function of incident P_{dyn} at each threshold altitude in Figure 7. The data points are color coded by the SZA value at density threshold 1 or 2. The data are binned by SZA using the same method as for

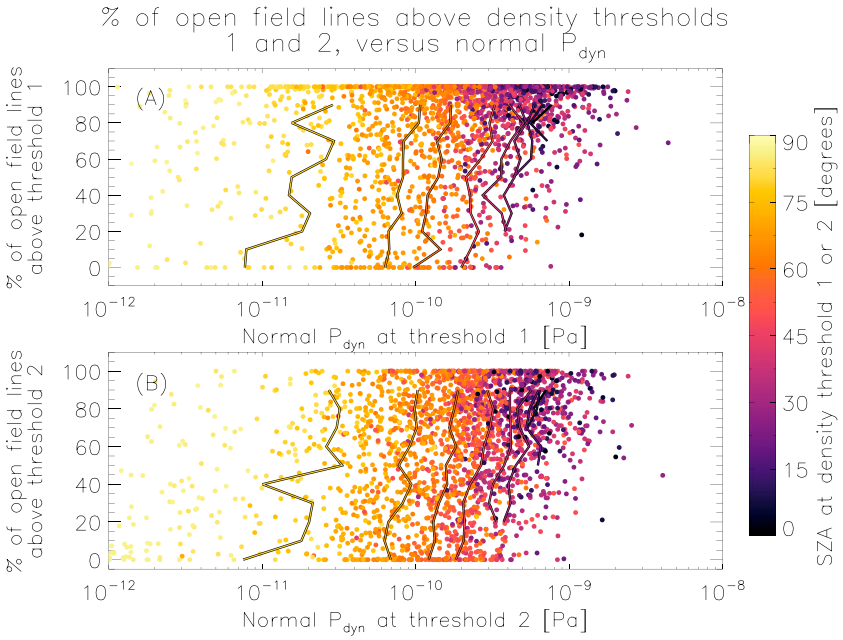

Figure 7. Percentage of open magnetic field lines observed above density thresholds 1 and 2 (panels A and B, respectively), as a function of incident dynamic pressure at threshold 1 or 2. Color denotes SZA at threshold 1 or 2. The solid lines show averages of data binned into overlapping 20°-sized SZA bins, with each bin centered at SZA values of 0° to 80° and spaced every 10°. SZA = solar zenith angle.

Figure 4. Large variability is again observed, but the percentage of open magnetic field lines above density thresholds 1 and 2 tends to increase as the incident P_{dyn} increases at each threshold altitude.

5. Discussion

5.1. The Importance of Open Magnetic Field Topology in the Upper Ionosphere

The individual altitude profiles shown in Figure 1 (along with many of the profiles inspected in this study that are not shown here) demonstrate that ionospheric density and magnetic topology is highly variable in the dayside Martian ionosphere, as has been previously reported (e.g., Withers, 2009). Figure 1D shows an example pass where the extent of the upper ionosphere appears to coincide with the transition from closed to open magnetic field topology. The statistical study reported here is an attempt to identify and quantify any correlations that exist between open magnetic field topology, the extent of the upper ionosphere, and the solar wind dynamic pressure normal to the dayside ionosphere. The large variability discussed above is the result of many drivers and parameters, including SZA, local magnetic field orientation (horizontal or vertical field), the presence (or lack there of) of crustal magnetic anomalies, seasonal effects (such as the solar photoionizing extreme ultraviolet irradiance), to name a few. We have attempted to control for the presence of crustal magnetic fields and SZA effects. The first is achieved by only analyzing orbits where the contribution from crustal magnetic anomalies at 400-km altitude is small (see section 3 for more information); the second is achieved by binning data as a function of SZA, as presented throughout section 4. Although large variability is still observed in the statistical analysis, clear trends emerge demonstrating the importance of the solar wind normal dynamic pressure and open magnetic field topology on the extent of the Martian upper ionosphere.

Figures 2 and 3 show to varying degrees that open magnetic field topology influences the altitudes of the 10^2 and 10^3 cm^{-3} density thresholds in the ionosphere, namely, that when a greater percentage of the magnetic field topology is open (vs. closed), the altitudes at which the ionospheric density drops below 10^2 and 10^3 cm^{-3} (density thresholds "1" and "2") decrease. This is most clearly shown in Figure 2A, where the altitude down to which open magnetic field topology reaches (the "topology transition altitude") and the altitude of density threshold 1 match almost 1:1. This suggests that the extent of the upper ionosphere (here defined to be when ionospheric density drops below 10^2 cm^{-3}) may be controlled by the transition from closed to open magnetic field. Such behavior may occur because the ionosphere is collisionless at the typical altitudes that the topology transition is observed at, meaning that planetary ions whose guiding centers are on open field lines just above this transition are more likely able to escape from this region and are thus not observed there. Planetary ions on closed magnetic field just below this transition are less likely to escape and are consequently observed there. The relatively minor response of density threshold 2 with respect to the topology transition altitude (panel B) suggests that this threshold may typically be located in the photochemically controlled region of the ionosphere, where processes in the upper ionosphere do not influence this region to a great extent.

The dependence of density threshold 1 (and to some extent 2) on SZA are not surprising, given that the dayside ionosphere is to first order controlled by the incident solar photoionizing flux, which decreases with increasing SZA. Similar trends concerning the main ionospheric peak have been reported in previous studies, and our results complement these earlier results (e.g., Fallows et al., 2015; Morgan et al., 2008; Vogt et al., 2017).

A range of separation altitudes between density thresholds 1 and 2 are observed, ranging from a sharp density drop-off with both thresholds located at the same altitude (0-km separation, to the accuracy of the 50-km bin sizes used) up to much smoother density drop-offs spanning separation altitudes of several hundred kilometers. Figures 3 and 5 suggest that the percentage of open field lines above density threshold 2, and the normal dynamic pressure, are important for determining this separation altitude. A greater percentage of open field lines observed above density threshold 2, and higher normal dynamic pressures, tends to coincide with smaller separation distances. The latter is particularly true at SZA greater than ~50° (see Figure 5), and may be because the separation distance is already small at lower SZA where the normal dynamic pressure is intrinsically larger and plasma boundaries tend to be sharper in general there.

When the separation distance between density thresholds 1 and 2 is relatively small, say less than ~100 km or so, the ionospheric density profile resembles that of an ionopause-like density profile. The ionopause

boundary is sometimes defined as a tangential discontinuity, across which the total pressure is constant and the normal components of the magnetic field and particle velocity are 0 (Schunk & Nagy, 2009). The ionopause boundary is typically observed at unmagnetized bodies when solar wind dynamic pressure is balanced by ionospheric thermal pressure above the exobase. It is a particularly prominent feature of the Venusian ionosphere at solar maximum and is characterized by a steep gradient in the ionospheric density as a function of altitude (e.g., Brace et al., 1980; Knudsen et al., 1979). The Venus ionopause is observed to broaden as it is pushed to lower altitudes by higher solar wind dynamic pressures (e.g., Elphic et al., 1981; Luhmann et al., 1987), a behavior thought to be related to the increasing effects of collisions. Several studies have identified the existence of an ionopause-like feature in the Martian ionosphere, although unlike at Venus, this feature only appears to be present for approximately half the time or less at Mars (Duru et al., 2009; Vogt et al., 2015). The inspection of many dayside passes by hand in this study (and those shown in Figure 1) revealed that sharp ionospheric density "ledges" are sometimes present and sometimes absent in the MAVEN data at Mars. The trends observed in Figures 3 and 5 may explain this, and the percentage of open magnetic field topology and the solar wind normal dynamic pressure may play an important role in determining when an ionopause-like feature is observed at Mars. Further investigation of this boundary was outside the topic of this study and was not followed further.

5.2. The Importance of Solar Wind Normal Dynamic Pressure for Open Magnetic Field Topology in the Upper Ionosphere

Case studies have shown that during times of extreme solar wind dynamic pressure, draped magnetic field lines are observed to penetrate deep into the Martian ionosphere (Xu et al., 2019; Xu, Fang, et al., 2018). The results of this study demonstrate similar behavior across the full range of solar wind normal dynamic pressures observed at Mars. Figure 2 demonstrates that the altitude of density threshold 1 matches almost 1:1 with the topology transition altitude, while Figure 4 shows that the altitudes of density thresholds 1 and 2 decrease as normal dynamic pressure increases. One can thus infer that the topology transition altitude will also decrease as normal dynamic pressure increases, and this is observed in Figure 6. A greater percentage of open and draped field lines are observed above both density thresholds under conditions of higher normal pressure, shown in Figure 7. One interpretation of this is that during times of lower normal dynamic pressure, there is more structure in the magnetic field topology above each density threshold, where closed, open, and draped fields may be observed. During times of strong normal dynamic pressure, this structure is compressed downward and replaced by mainly draped field above the density thresholds, as shown in Figure 7.

An important caveat to remember in the interpretation of the presented observations is that MAVEN possesses a significant horizontal velocity in the ionosphere and the profiles shown are not true vertical profiles. It is likely that the spacecraft crosses different spatial structures and observes time variability within a single pass, which likely determine whether MAVEN observes open or closed magnetic field at any given measurement point.

A recent study by Ramstad et al. (2018) analyzed 10 years of Mars EXpress ion data and found that heavy ion escape rates decreased slightly, with increasing solar wind dynamic pressure, opposite to the inferences drawn in this study. It is not yet clear why this discrepancy exists between these two studies; however, comparison of the analysis methods may help explain and consolidate these differences. The Ramstad et al. (2018) study analyzed heavy ion fluxes mostly in the tail region, and to first order did not include ions escaping in the polar plume region. The authors note that ion escape in the polar plume could become enhanced during times of stronger dynamic pressure, offsetting the observed decreases in tail escape. Additionally, our study analyzed the response of Martian magnetic topology to changes in the normal dynamic pressure, which is strongly dependent on the SZA at each measurement point, as shown in Figures 1B and 1F. The Ramstad et al. (2018) study did not take into account SZA and analyzed heavy ion escape rates with respect to upstream solar wind dynamic pressure only.

5.3. Extreme Solar Wind Dynamic Pressures at Mars in the Context of This Study

MAVEN has been at Mars since September 2014, toward the end of the maximum activity phase of solar cycle 24. Because of the overall weaker interplanetary conditions in the heliosphere during cycle 24, in comparison to the previous cycle, the strength and occurrence of high dynamic pressure events (such as CMEs) has been moderate during this time period (Lee et al., 2017, 2018). To put into context the upstream dynamic pressure values associated with these high dynamic pressure events, namely, those triggered by CMEs and high speed solar wind streams, with those that were measured during quiet solar wind conditions,

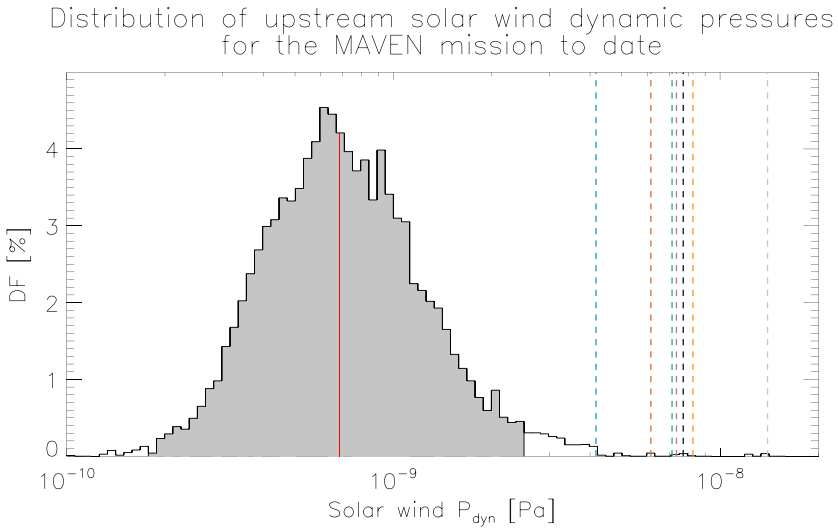

Figure 8. Distribution of all upstream solar wind dynamic pressures observed by MAVEN. The gray shaded area denotes the 97.5th percentile, and the solid red vertical line marks the median value of the data set. The dashed vertical lines mark the seven space weather events observed by MAVEN (left to right). Brown: 4 March 2015; orange: 8 March 2015; purple: 13 January 2016; green: 7 June 2016; black: 17 September 2016; gray: 22 June 2015; blue: 13 September 2017. MAVEN = Mars Atmosphere and Volatile EvolutioN; DF = Distribution function.

the distribution of all upstream solar wind dynamic pressures observed by MAVEN is shown in Figure 8. The shaded gray area marks the 97.5th percentile, and the dashed colored vertical lines mark seven upstream dynamic pressure values measured by MAVEN, which are associated with these space weather events. The dates of these events are given in the figure caption. These are quite clearly extremes and lie a factor of ∼10 or more above the median dynamic pressure value (marked as the solid red vertical line). A comparison to Figures 4 to 7 from this study suggest that draped magnetic field should penetrate deep into the ionosphere during these extreme events, down to 200-km altitude or below. Such behavior would likely contribute to the observed enhanced ionospheric escape rates during these space weather event periods.

Unfortunately, observing conditions during all of these extreme dynamic pressure events were not ideal and have made it difficult to fully characterize the ionospheric responses: MAVEN's periapsis was located close to or even past the terminator for some events, and/or extreme spacecraft charging during periapsis significantly degraded the plasma data. The only event that shows some promise is the 13 September 2017 event (the blue line), where MAVEN's periapsis was located at about 70° SZA. An overview of this CME event has been provided by Lee et al. (2018); significant spacecraft charging is still present below 200-km altitude during this event, but a future study none the less aims to fully characterize the ionospheric response.

We end our discussion with some comments regarding the ongoing evaluation of the evolution of Mars' atmosphere over time and how the results presented in this study may provide some insight (or perhaps additional complexities) to this evaluation. The young Sun is thought to have been significantly more active than today, with a quiet time solar wind perhaps 2–3 times denser and faster than today's quiet time values (e.g., Boesswetter et al., 2010; Newkirk Jr, 1980; Ribas et al., 2005). The corresponding solar wind dynamic pressure (and normal dynamic pressure) would subsequently be at least a factor of 10 or so greater than the quiet time value today, meaning that typical solar wind conditions for past Mars may have been equivalent to the extreme dynamic pressure events observed today. If one assumes that the neutral atmosphere and ionosphere at past Mars are the same as today (which is probably not a good assumption due to higher solar extreme ultraviolet irradiance [Tu et al., 2015]), then ionospheric escape to space may have been greatly enhanced in the past, given the deep penetration of draped magnetic field lines that we would expect, based on the results of this study. Mars is thought to have possessed a substantially thicker atmosphere in its past (e.g., Carr, 1983, 1999; Kasting, 1991), and further work is needed to quantify how such an atmosphere may affect the results of this study.

6. Conclusions

Open and draped magnetic field line topologies are thought to be an important enabler of ionospheric escape to space at Mars, providing ionospheric particles access to the solar wind. A statistical study of 4 years of MAVEN dayside ionospheric data shows that open and draped field lines penetrate deeper into the ionosphere during conditions of enhanced upstream solar wind dynamic pressure. Additionally, the altitudes at which the ionospheric density drops below 10^2 and 10^3 cm^{-3} are also observed at decreasing altitudes, under increasing dynamic pressures normal to the atmosphere. The altitude of the 10^2 cm^{-3} density threshold to first order coincides with the altitude down to which open and draped magnetic fields penetrate, demonstrating that times of enhanced solar wind normal dynamic pressure likely produce enhancements of ionospheric escape to space as a result of this deeper penetration of open and draped fields into the ionosphere.

The early Sun is thought to have a possessed a denser, faster solar wind, producing a typical dynamic pressure at least ~10 times greater than today's typical conditions. Quiet time conditions for past Mars may have been equivalent to extreme dynamic pressure events today, and draped magnetic fields may have been able to penetrate deeply into the ionosphere on a regular basis. Ionospheric escape to space may thus have been an important mechanism for atmospheric loss to space and evolution over the planets history. A better understanding of Mars' past atmospheric and ionospheric conditions are needed before quantitative evaluations can be made.

Acknowledgments
Work at LASP and SSL was supported by NASA funding for the MAVEN project through the Mars Exploration Program under grant NNH10CC04C. Data used in this study are available on the NASA Planetary Data System (https://pds.nasa.gov/).

References

Acuna, M., Connerney, J., Lin, R., Mitchell, D., Carlson, C., McFadden, J., et al. (1999). Global distribution of crustal magnetization discovered by the Mars Global Surveyor MAG/ER experiment. *Science*, *284*(5415), 790–793.

Andersson, L., Ergun, R., Delory, G., Eriksson, A., Westfall, J., Reed, H., et al. (2015). The Langmuir probe and waves (LPW) instrument for MAVEN. *Space Science Reviews*, *195*(1-4), 173–198.

Bertucci, C., Duru, F., Edberg, N., Fraenz, M., Martinecz, C., Szego, K., & Vaisberg, O. (2011). The induced magnetospheres of Mars, Venus, and Titan. *Space Science Reviews*, *162*(1-4), 113–171.

Boesswetter, A., Lammer, H., Kulikov, Y., Motschmann, U., & Simon, S. (2010). Non-thermal water loss of the early Mars: 3D multi-ion hybrid simulations. *Planetary and Space Science*, *58*(14-15), 2031–2043.

Brace, L. H., Theis, R. F., Hoegy, W. R., Wolfe, J. H., Mihalov, J. D., Russell, C. T., et al. (1980). The dynamic behavior of the Venus ionosphere in response to solar wind interactions. *Journal of Geophysical Research*, *85*(A13), 7663–7678. https://doi.org/10.1029/JA085iA13p07663

Brain, D. A., Bagenal, F., Acua, M. H., & Connerney, J. E. P. (2003). Martian magnetic morphology: Contributions from the solar wind and crust. *Journal of Geophysical Research*, *108*(A12), 1424. https://doi.org/10.1029/2002JA009482

Brain, D., Lillis, R., Mitchell, D., Halekas, J., & Lin, R. (2007). Electron pitch angle distributions as indicators of magnetic field topology near Mars. *Journal of Geophysical Research*, *112*, A09201. https://doi.org/10.1029/2007JA012435

Breus, T., Bauer, S., Krymskii, A., & Mitnitskii, V. Y. (1989). Mass loading in the solar wind interaction with Venus and Mars. *Journal of Geophysical Research*, *94*(A3), 2375–2382.

Carr, M. H. (1983). Stability of streams and lakes on Mars. *Icarus*, *56*(3), 476–495.

Carr, M. H. (1999). Retention of an atmosphere on early Mars. *Journal of Geophysical Research*, *104*(E9), 21,897–21,909.

Chaffin, M. S., Chaufray, J.-Y., Deighan, J., Schneider, N. M., Mcclintock, W. E., Stewart, A. I. F., et al. (2015). Three-dimensional structure in the Mars H corona revealed by IUVS on MAVEN. *Geophysical Research Letters*, *42*, 9001–9008. https://doi.org/10.1002/2015GL065287

Connerney, J., Espley, J., DiBraccio, G., Gruesbeck, J., Oliversen, R., Mitchell, D., et al. (2015). First results of the MAVEN magnetic field investigation. *Geophysical Research Letters*, *42*, 8819–8827. https://doi.org/10.1002/2015GL065366

Curry, S. M., Luhmann, J. G., Ma, Y. J., Dong, C. F., Brain, D., Leblanc, F., et al. (2015). Response of Mars O^+ pickup ions to the 8 March 2015 ICME: Inferences from MAVEN data-based models. *Geophysical Research Letters*, *42*, 9095–9102. https://doi.org/10.1002/2015GL065304

Dubinin, E., & Lundin, R. (1995). Mass-loading near Mars. *Advances in Space Research*, *16*(4), 75–79.

Duru, F., Gurnett, D., Frahm, R., Winningham, J., Morgan, D., & Howes, G. (2009). Steep, transient density gradients in the Martian ionosphere similar to the ionopause at Venus. *Journal of Geophysical Research*, *114*, A10316. https://doi.org/10.1029/2009JA014711

Edberg, N. J. T., Nilsson, H., Williams, A. O., Lester, M., Milan, S. E., Cowley, S. W. H., et al. (2010). Pumping out the atmosphere of Mars through solar wind pressure pulses. *Geophysical Research Letters*, *37*, L03107. https://doi.org/10.1029/2009GL041814

Elphic, R., Russell, C., Luhmann, J., Scarf, F., & Brace, L. (1981). The Venus ionopause current sheet: Thickness length scale and controlling factors. *Journal of Geophysical Research*, *86*(A13), 11,430–11,438.

Ergun, R., Morooka, M., Andersson, L., Fowler, C., Delory, G., Andrews, D. J., et al. (2015). Dayside electron temperature and density profiles at Mars: First results from the MAVEN Langmuir probe and waves instrument. *Geophysical Research Letters*, *42*, 8846–8853. https://doi.org/10.1002/2015GL065280

Fallows, K., Withers, P., & Matta, M. (2015). An observational study of the influence of solar zenith angle on properties of the M1 layer of the Mars ionosphere. *Journal of Geophysical Research: Space Physics*, *120*, 1299–1310. https://doi.org/10.1002/2014JA020750

Fowler, C. M., Andersson, L., Halekas, J., Espley, J. R., Mazelle, C., Coughlin, E. R., et al. (2017). Electric and magnetic variations in the near-Mars environment. *Journal of Geophysical Research: Space Physics*, *122*, 8536–8559. https://doi.org/10.1002/2016JA023411

Futaana, Y., Barabash, S., Yamauchi, M., McKenna-Lawlor, S., Lundin, R., Luhmann, J., et al. (2008). Mars Express and Venus Express multi-point observations of geoeffective solar flare events in December 2006. *Planetary and Space Science*, *56*(6), 873–880.

Halekas, J., Brain, D., Luhmann, J., DiBraccio, G., Ruhunusiri, S., Harada, Y., et al. (2017a). Flows, fields, and forces in the Mars-solar wind interaction. *Journal of Geophysical Research: Space Physics*, *122*, 11,320–11,341. https://doi.org/10.1002/2017JA024772

Halekas, J., Lillis, R., Mitchell, D., Cravens, T., Mazelle, C., Connerney, J., et al. (2015b). MAVEN observations of solar wind hydrogen deposition in the atmosphere of Mars. *Geophysical Research Letters*, *42*, 8901–8909. https://doi.org/10.1002/2015GL064693

Halekas, J., Ruhunusiri, S., Harada, Y., Collinson, G., Mitchell, D., Mazelle, C., et al. (2017b). Structure, dynamics, and seasonal variability of the Mars-solar wind interaction: MAVEN Solar Wind Ion Analyzer in-flight performance and science results. *Journal of Geophysical Research: Space Physics*, *122*, 547–578. https://doi.org/10.1002/2016JA023167

Halekas, J., Taylor, E., Dalton, G., Johnson, G., Curtis, D., McFadden, J., et al. (2015a). The solar wind ion analyzer for MAVEN. *Space Science Reviews*, *195*(1-4), 125–151.

Holmström, M. (2006). Asymmetries in Mars' exosphere. *Space Science Reviews*, *126*(1-4), 435–445.

Jakosky, B. M., Grebowsky, J. M., Luhmann, J. G., Connerney, J., Eparvier, F., Ergun, R., et al. (2015a). MAVEN observations of the response of Mars to an interplanetary coronal mass ejection. *Science*, *350*(6261), aad0210.

Jakosky, B. M., Lin, R., Grebowsky, J., Luhmann, J., Mitchell, D., Beutelschies, G., et al. (2015b). The Mars Atmosphere and Volatile EvolutioN (MAVEN) mission. *Space Science Reviews*, *195*(1-4), 3–48.

Jakosky, B. M., Slipski, M., Benna, M., Mahaffy, P., Elrod, M., Yelle, R., et al. (2017). Mars atmospheric history derived from upper-atmosphere measurements of 38Ar/36Ar. *Science*, *355*(6332), 1408–1410.

Kasting, J. F. (1991). CO_2 condensation and the climate of early Mars. *Icarus*, *94*(1), 1–13.

Knudsen, W., Spenner, K., Whitten, R., Spreiter, J., Miller, K., & Novak, V. (1979). Thermal structure and major ion composition of the Venus ionosphere: First RPA results from Venus orbiter. *Science*, *203*(4382), 757–763.

Lee, C., Hara, T., Halekas, J., Thiemann, E., Chamberlin, P., Eparvier, F., et al. (2017). MAVEN observations of the solar cycle 24 space weather conditions at Mars. *Journal of Geophysical Research: Space Physics*, *122*, 2768–2794. https://doi.org/10.1002/2016JA023495

Lee, C., Jakosky, B., Luhmann, J., Brain, D., Mays, M., Hassler, D., et al. (2018). Observations and impacts of the 10 September 2017 solar events at Mars: An overview and synthesis of the initial results. *Geophysical Research Letters*, *45*, 8871–8885. https://doi.org/10.1029/2018GL079162

Luhmann, J., Dong, C., Ma, Y., Curry, S., Xu, S., Lee, C., et al. (2017). Martian magnetic storms. *Journal of Geophysical Research: Space Physics*, *122*, 6185–6209. https://doi.org/10.1002/2016JA023513

Luhmann, J. G., Russell, C. T., Scarf, F. L., Brace, L. H., & Knudsen, W. C. (1987). Characteristics of the Marslike limit of the Venus-solar wind interaction. *Journal of Geophysical Research*, *92*(A8), 8545–8557. https://doi.org/doi:10.1029/JA092iA08p08545

Lundin, R., Barabash, S., Fedorov, A., Holmström, M., Nilsson, H., Sauvaud, J.-A., & Yamauchi, M. (2008). Solar forcing and planetary ion escape from Mars. *Geophysical Research Letters*, *35*, L09203. https://doi.org/10.1029/2007GL032884

Ma, Y. J., Fang, X., Nagy, A. F., Russell, C. T., & Toth, G. (2014). Martian ionospheric responses to dynamic pressure enhancements in the solar wind. *Journal of Geophysical Research: Space Physics*, *119*, 1272–1286. https://doi.org/10.1002/2013JA019402

Ma, Y., Russell, C., Fang, X., Dong, C., Nagy, A., Toth, G., et al. (2017). Variations of the Martian plasma environment during the ICME passage on 8 March 2015: A time-dependent MHD study. *Journal of Geophysical Research: Space Physics*, *122*, 1714–1730. https://doi.org/10.1002/2016JA023402

Marquette, M. L., Lillis, R. J., Halekas, J., Luhmann, J., Gruesbeck, J., & Espley, J. (2018). Autocorrelation study of solar wind plasma and IMF properties as measured by the MAVEN spacecraft. *Journal of Geophysical Research: Space Physics*, *123*, 2493–2512. https://doi.org/10.1002/2018JA025209

Mitchell, D., Mazelle, C., Sauvaud, J.-A., Thocaven, J.-J., Rouzaud, J., Fedorov, A., et al. (2016). The MAVEN solar wind electron analyzer. *Space Science Reviews*, *200*(1-4), 495–528.

Morgan, D. D., Gurnett, D. A., Kirchner, D. L., Fox, J. L., Nielsen, E., & Plaut, J. J. (2008). Variation of the Martian ionospheric electron density from Mars Express radar soundings. *Journal of Geophysical Research*, *113*, A09303. https://doi.org/10.1029/2008JA013313

Morschhauser, A., Lesur, V., & Grott, M. (2014). A spherical harmonic model of the lithospheric magnetic field of Mars. *Journal of Geophysical Research: Planets*, *119*, 1162–1188. https://doi.org/10.1002/2013JE004555

Newkirk Jr, G. (1980). Solar variability on time scales of 10 to the 5th years to 10 to the 9.6th years, *The Ancient Sun: Fossil record in the Earth, Moon and meteorites* pp. 293–320). New York and Oxford: Pergamon Press.

Opgenoorth, H. J., Andrews, D. J., Fränz, M., Lester, M., Edberg, N. J. T., Morgan, D., et al. (2013). Mars ionospheric response to solar wind variability. *Journal of Geophysical Research: Space Physics*, *118*, 6558–6587. https://doi.org/10.1002/jgra.50537

Rahmati, A., Larson, D., Cravens, T., Lillis, R., Dunn, P., Halekas, J., et al. (2015). MAVEN insights into oxygen pickup ions at Mars. *Geophysical Research Letters*, *42*, 8870–8876. https://doi.org/10.1002/2015GL065262

Ramstad, R., Barabash, S., Futaana, Y., Nilsson, H., & Holmström, M. (2018). Ion escape from mars through time: An extrapolation of atmospheric loss based on 10 years of Mars Express measurements. *Journal of Geophysical Research: Planets*, *123*, 3051–3060. https://doi.org/10.1029/2018JE005727

Ribas, I., Guinan, E. F., Güdel, M., & Audard, M. (2005). Evolution of the solar activity over time and effects on planetary atmospheres. I. High-energy irradiances (1–1700 Å). *The Astrophysical Journal*, *622*(1), 680.

Schunk, R., & Nagy, A. (2009). *Ionospheres: Physics, plasma physics, and chemistry*. Cambridge: Cambridge university press.

Tu, L., Johnstone, C. P., Güdel, M., & Lammer, H. (2015). The extreme ultraviolet and X-ray Sun in Time: High-energy evolutionary tracks of a solar-like star. *Astronomy & Astrophysics*, *577*, L3.

Vogt, M. F., Withers, P., Fallows, K., Andersson, L., Girazian, Z., Mahaffy, P. R., et al. (2017). MAVEN observations of dayside peak electron densities in the ionosphere of Mars. *Journal of Geophysical Research: Space Physics*, *122*, 891–906. https://doi.org/10.1002/2016JA023473

Vogt, M. F., Withers, P., Mahaffy, P. R., Benna, M., Elrod, M. K., Halekas, J. S., et al. (2015). Ionopause-like density gradients in the Martian ionosphere: A first look with MAVEN. *Geophysical Research Letters*, *42*, 8885–8893. https://doi.org/10.1002/2015GL065269

Weber, T., Brain, D., Mitchell, D., Xu, S., Connerney, J., & Halekas, J. (2017). Characterization of low-altitude nightside Martian magnetic topology using electron pitch angle distributions. *Journal of Geophysical Research: Space Physics*, *122*, 9777–9789. https://doi.org/10.1002/2017JA024491

Withers, P. (2009). A review of observed variability in the dayside ionosphere of Mars. *Advances in Space Research*, *44*(3), 277–307.

Xu, S., Curry, S. M., Mitchell, D. L., Luhmann, J. G., Lillis, R. J., & Dong, C. (2019). Magnetic topology response to the 2003 Halloween ICME event at Mars. *Journal of Geophysical Research: Space Physics*, *124*, 151–165. https://doi.org/10.1029/2018JA026118

Xu, S., Fang, X., Mitchell, D. L., Ma, Y., Luhmann, J. G., DiBraccio, G. A., et al. (2018). Investigation of Martian magnetic topology response to 2017 September ICME. *Geophysical Research Letters*, *45*, 7337–7346. https://doi.org/10.1029/2018GL077708

Xu, S., Liemohn, M., Bougher, S., & Mitchell, D. (2015). Enhanced carbon dioxide causing the dust storm-related increase in high-altitude photoelectron fluxes at Mars. *Geophysical Research Letters*, *42*, 9702–9710. https://doi.org/10.1002/2015GL066043

Xu, S., Mitchell, D., Liemohn, M., Fang, X., Ma, Y., Luhmann, J., et al. (2017). Martian low-altitude magnetic topology deduced from MAVEN/SWEA observations. *Journal of Geophysical Research: Space Physics*, *122*, 1831–1852. https://doi.org/10.1002/2016JA023467

Xu, S., Weber, T., Mitchell, D. L., Brain, D. A., Mazelle, C., DiBraccio, G. A., & Espley, J. (2018). A technique to infer magnetic topology at Mars and its application to the terminator region. *Journal of Geophysical Research: Space Physics*, *0*. https://doi.org/10.1029/2018JA026366

Zhang, M. H. G., & Luhmann, J. G. (1992). Comparisons of peak ionosphere pressures at Mars and Venus with incident solar wind dynamic Pressure. *Journal of Geophysical Research*, *97*(E1), 1017–1025. https://doi.org/10.1029/91JE02721